

Ab Initio Calculation of Crystalline Electric Fields and Kondo Temperatures in Ce-Compounds

J. E. Han^{a,b}, M. Alouani^a, and D. L. Cox^{a,b}

^a-Department of Physics, The Ohio State University, Columbus, Ohio 43210

^b-Institute for Theoretical Physics, University of California, Santa Barbara 93106-4030

Abstract

We have calculated the band- f hybridizations for $\text{Ce}_x\text{La}_{1-x}\text{M}_3$ compounds ($x = 1$ and $x \rightarrow 0$; $\text{M}=\text{Pb, In, Sn, Pd}$) within the local density approximation and fed this into a non-crossing approximation for the Anderson impurity model applied to both dilute and concentrated limits. Our calculations produce crystalline electric field splittings and Kondo temperatures with trends in good agreement with experiment and demonstrate the need for detailed electronic structure information on hybridization to describe the diverse behaviors of these Ce compounds.

75.30.Mb, 71.27.+a, 75.10.Dg

A pressing issue in the understanding of strongly interacting electronic materials is how to produce realistic theoretical descriptions which encompass both crystalline environment and symmetry effects, well treated by *ab initio* electronic structure theory, with dynamical effects best treated within many body formalisms. A case in point is heavy fermion materials with strongly interacting f -electron states that give rise to huge electronic mass enhancements. Some understanding of these systems has been reached in Anderson model approaches which assume a nearly atomic limit picture for f -states that hybridize with extended conduction states through matrix elements determined from electronic structure (local density approximation or LDA) calculations [1–5]. In particular, Gunnarsson and Schöhammer [1], have calculated high energy spectra for a number of cerium based metals with a $T = 0$ variational method, which however ignored crystal field effects. The LDA has been used to estimate hybridization induced crystalline electric field (CEF) splittings in cerium systems [3] without including the strong correlation effects which give rise to the Kondo effect screening of the f -electron magnetic moments by itinerant electrons. Second order perturbation theory in the direct Coulomb interaction strength U has been employed, and this gives good estimates for electron mass enhancements while only partially capturing Kondo effect physics [5].

In this work, we present first results for a method which combines a nonperturbative, finite temperature diagrammatic approach for the Anderson model (the Non-Crossing Approximation) with input parameters from the LDA. The NCA can properly generate hybridization induced CEF splittings while giving an excellent description of the Kondo effect. We report calculations of the CEF splittings and Kondo scales T_K in CeM_3 ($\text{M}=\text{Pb}, \text{In}, \text{Sn}, \text{Pd}$) compounds in which experimental T_K values vary with M by nearly three orders of magnitude. We have computed energy dependent hybridization matrix elements between Ce f -states and other conduction states within the LDA in two limits:

- 1) For the dilute alloy system $\text{Ce}_x\text{La}_{1-x}\text{M}_3$ with $x \rightarrow 0$;
- 2) For concentrated CeM_3 compounds.

We explain and compare the methods and results of those approaches. We correctly find a

stable Γ_7 doublet CEF ground state with small T_K values for CePb₃ and CeIn₃ and large T_K values with negligible CEF effects for CeSn₃ and CePd₃.

In our work, the CEF splittings are induced by band- f hybridization, which is anticipated to be the dominant contribution [4]. This splitting arises as follows: a CEF state in Ce- f^1 configuration is shifted downward by level repulsion through virtual $f^1 \rightarrow f^0 \rightarrow f^1$ and $f^1 \rightarrow f^2 \rightarrow f^1$ charge fluctuations. In the presence of crystalline anisotropy, different irreducible representations (irreps) of the point group in the f^1 manifold receive different shifts. Using this idea in second order perturbation theory, Wills and Cooper [3] estimated the contribution of the hybridization-induced CEF splittings on top of extrapolated point charge contributions [6]. Although the electrostatic potential from the cubic environment can induce the CEF (*i.e.*, in the point charge model [6]), it is difficult to produce a good estimate of this contribution in a metal due to conduction electron charge screening [6] and metallic covalency. We shall neglect point charge contributions in this letter.

We describe the Ce_xLa_{1-x}M₃ systems in terms of effective impurity Anderson models [17,18] in the dilute ($x \rightarrow 0$) and concentrated ($x = 1$) limits at a site of cubic symmetry relevant to the Cu₃Au structure. In this Letter, we ignore intersite interaction effects such as the anti-ferromagnetism found in CeIn₃ [16] and CePb₃ [17]. The impurity Anderson Hamiltonian of interest reads

$$H = \sum_{\mathbf{k}\sigma} \epsilon_{\mathbf{k}\sigma} c_{\mathbf{k}\sigma}^\dagger c_{\mathbf{k}\sigma} + \frac{1}{\sqrt{N_s}} \sum_{\mathbf{k}\sigma, m} (V_{\mathbf{k}\sigma m} c_{\mathbf{k}\sigma} f_m^\dagger + h.c.) + \sum_m \epsilon_{fm} f_m^\dagger f_m + U \sum_{m < m'} n_{fm} n_{fm'}, \quad (1)$$

where m is the label of cubic irrep states, *e.g.* $m = |J = \frac{5}{2}; \Gamma_{7+}\rangle$, $V_{\mathbf{k}\sigma m}$ the hopping matrix element between conduction electron ($c_{\mathbf{k}\sigma}$) and f -orbital (f_m), N_s the number of sites, ϵ_{fm} the f -level energy measured from the Fermi level, U the on-site Coulomb repulsion between two f -electrons.

We have used $\epsilon_{fm} = -2.0$ eV for Hund's ground multiplet ($J=5/2$) in all the calculations, consistent with experimental [7] and theoretical [8,9] values. The spin-orbit (SO) splitting Δ_{SO} was read off from the separation between $J = 5/2$ and $J = 7/2$ peaks in the Ce

4*f* projected densities of states (DOS). We find $\Delta_{\text{SO}} = 0.35$ eV for all M, in agreement with atomic values. We set the onsite Coulomb repulsion $U \rightarrow \infty$ in our many body approximation, though we partially correct for this as we shall describe below. In the cubic point group symmetry of the CeM_3 compounds, the $J = \frac{5}{2}$ multiplet decomposes into a Γ_7 magnetic doublet ($|\frac{5}{2}; \Gamma_7\rangle$) and Γ_8 quartet ($|\frac{5}{2}; \Gamma_8\rangle$), split by an energy Δ_{78} . The $J = \frac{7}{2}$ multiplet splits into Γ_6 and Γ_7 doublets, and a Γ_8 quartet. Experimentally, the Γ_7 doublet lies lowest for M=Pb, In ($\Delta_{78} > 0$), while no CEF splitting is resolved for M=Sn, Pd.

The hybridization matrix elements are calculated from the LDA using the Linearized Muffin-Tin orbital (LMTO) method in the Atomic Sphere Approximation (ASA) including the so called combined correction term [10]. We assumed the same Wigner-Seitz radii for Ce and M (=Pb, In, Sn) and used experimental lattice constants. For CePd_3 , the Wigner-Seitz radius of Ce was set to be 10 % larger than that of Pd [11]. We used 165 \mathbf{k} -points in the irreducible Brillouin zone for the self-consistent solution with DOS integrations carried out using the tetrahedron method [13]. We set the orbital basis as s, p, d, f for Ce and s, p, d for M-ligands.

In the concentrated limit ($x \rightarrow 1$, *i.e.*, CeM_3), we define the hybridization $\Gamma_{mm'}^{\text{med}}(\epsilon)$, in terms of an effective *impurity* Anderson model, with the hybridization derived from the overlap between f -orbital at the origin and the rest of the lattice. (See FIG. 1 (a) and FIG. 2 (a)) More specifically

$$\Gamma_{mm'}^{\text{med}}(\epsilon) = -\text{Im} \sum_{\mathbf{R}, \mathbf{R}'} V_{\mathbf{R}m} V_{\mathbf{R}'m'}^* G'(\mathbf{R}, \mathbf{R}', \epsilon + i\eta), \quad (2)$$

where $V_{\mathbf{R}m}$ is the hopping matrix element between m -th f -orbital and ligand orbital at \mathbf{R} and $G'(\mathbf{R}, \mathbf{R}', \epsilon + i\eta)$ the Greens' function of ligand electron created at \mathbf{R} and recovered at \mathbf{R}' , with the central f -orbital excluded, as shown in FIG. 1 (a). Now the array of ligand- and origin excluded f -orbitals (with origin excluded) serves as an effective *static* medium coupled to the f -orbital at the origin. Our method follows Gunnarsson *et. al.*'s suggestion [14] to interpret the f -projected DOS as the spectral function of an effective *non-interacting* resonant level model. This corresponds to the first iteration of a “dynamical mean field

theory” or “local approximation” to the interacting problem [15], which becomes exact in infinite spatial dimensions. We obtain the hybridization through Hilbert transformation as follows:

$$\begin{aligned}\Gamma_{mm'}^{\text{med}}(\epsilon) &= -\frac{i}{2} \left(\mathbf{G}^{LDA}(\epsilon + i\eta)^{-1} - \mathbf{G}^{LDA}(\epsilon - i\eta)^{-1} \right)_{mm'} \\ G_{mm'}^{LDA}(\epsilon \pm i\eta) &= \int dz \frac{\rho_{mm'}^{LDA}(z)}{\epsilon \pm i\eta - z},\end{aligned}\tag{3}$$

where $G_{mm'}^{LDA}(\epsilon \pm i\eta)$ is the 14×14 matrix Green’s function, $\rho_{mm'}^{LDA}(\epsilon)$ the f -PDOS derived from the band calculation with the LDA. We display the calculated $x \rightarrow 1$ limit model hybridization in FIG. 2 (a).

In the impurity limit ($x \rightarrow 0$), we calculate the hybridization between f and *bare* ligands, that is,

$$\Gamma_{mm'}^{\text{imp}}(\epsilon) = \pi \sum_{\mathbf{k}\sigma} V_{\mathbf{k}\sigma m}^* V_{\mathbf{k}\sigma m'} \delta(\epsilon - \epsilon_{\mathbf{k}\sigma}).\tag{4}$$

While, in the concentrated limit, the f -electron hops into already-formed bonding states of f (origin excluded)-ligand, this impurity limit hybridization accounts for the overlap of f and pre-bonding ligand states. (See FIG. 1 (b) and FIG. 2 (b)) Although this hybridization is calculated for a *lattice* Anderson Hamiltonian, we can still apply it to impurity limit of $\text{Ce}_x\text{La}_{1-x}\text{M}_3$ since the Ce-Ce hopping is negligibly small [12]. The procedure for computing $V_{\mathbf{k}\sigma m}$ is to set up a resonant level *lattice* model Hamiltonian matrix from the highly non-orthogonal basis of linear muffin-tin orbitals. We reconstruct the Hamiltonian from eigenvectors and eigenvalues of the LMTO equation in the *one-center* expression [10]. Hence, in the one-center basis, the angular momentum states become trivially orthogonal. After diagonalizing the ligand sector of the matrix and applying a suitable unitary transformation to the new ligand basis, we can directly read off hybridization matrix elements, $V_{\mathbf{k}\sigma m}$. To compute $\Gamma_{mm'}^{\text{imp}}(\epsilon)$, the Brillouin Zone sum of Eq. (4) is calculated with the tetrahedra method [13]. In this limit, we used lattice constants of LaM_3 compounds and readjusted the Fermi energy such that the ligand bands are filled up with $N_{\text{total}} - 1$ electrons (which accounts for the lattice-wide removal of the single Ce $4f^1$ electron).

As seen in FIG. 2, the $x \rightarrow 0$ and $x \rightarrow 1$ limit hybridizations are almost identical in the high energy region ($|\epsilon - E_F| \geq 0.5$ eV). In the low energy region (inset), the peak at -0.1 eV in the impurity limit (FIG. 2 (a)) is pushed down to -0.2 eV in the effective medium hybridization due to the bonding of Ce- f and Pb- p orbitals. Since the Kondo temperatures (T_K) depend upon the hybridization weight below the Fermi energy (E_F), this bonding effect can lead to a completely different scale of T_K as x changes. For CePb₃ [17] and CeSn₃ [18] experimental T_K values are constant with x , and our calculations (Table 1) show this within reasonable accuracy, given the exponential sensitivity of T_K to model parameters [19]. Another difference between the $x \rightarrow 0$ and $x \rightarrow 1$ limits is the extra structure appearing in the $x \rightarrow 1$ calculation above E_F (dashed line of FIG. 1(a)) which is due to flat f -bands. Although this feature above E_F is qualitatively different from the $x \rightarrow 0$ limit, it contributes little to Δ_{78} .

We solved the $U \rightarrow \infty$ Anderson model by using the well known Non-Crossing Approximation (NCA) which gives a good quantitative description of Ce compounds except for $T \leq T_p \ll T_K$ (where T_p is a “pathology scale” signalling breakdown of the approximation) [2]. To the first order expansion in $1/N_g$, with N_g the ground multiplet degeneracy, the spectral functions of the f^0 and f^1 states are solved for from coupled self consistent non-linear integral equations for the f^0, f^1 self energies. To partially correct for our $U \rightarrow \infty$ approximation, we have estimated the contribution to Δ_{78} arising from virtual f^2 occupancy between $|\frac{5}{2}; \Gamma_7\rangle$ and $|\frac{5}{2}; \Gamma_8\rangle$ by employing second order perturbation theory with $U = 6$ eV. We then added the resulting shifts to the *bare* f -level positions in the NCA. Δ_{78} values were inferred as the peak position separations between $|\frac{5}{2}; \Gamma_7\rangle$ and $|\frac{5}{2}; \Gamma_8\rangle$ f^1 spectral functions, which include contributions to all orders in V^2 , as per Levy and Zhang [4] and in contrast to Wills and Cooper [3]. The Kondo temperatures T_K were interpreted as the low temperature splitting between the f^0 spectral peak and the peak of the lowest f^1 CEF state spectrum. T_K roughly depends upon the hybridization strengths as [20]

$$T_K \approx D_{eff} \left(\frac{\Gamma_g}{\pi|\epsilon_f|} \right)^{\frac{1}{N_g}} \left(\frac{D_{eff}}{\Delta_{78}} \right)^{\frac{N_{ex}}{N_g}} \exp \left(\frac{\pi\epsilon_f}{N_g\Gamma_g} \right), \quad (5)$$

where D_{eff} is the effective band width, Γ_g hybridization strength at Fermi energy for ground multiplet, and $N_g(N_{ex})$ the degeneracy of ground(excited) multiplets.

The CeM_3 compounds ($\text{M}=\text{Pb, In, Sn}$) have the doublet ($|\frac{5}{2}; \Gamma_7\rangle$) states as the lowest lying multiplet with Δ_{78} values in good agreement with the experiments [16–18], as listed in Table 1. For the heavy fermion systems CeIn_3 and CePb_3 , $\Delta_{78} > 0$ (Γ_7 is stable) and $\Delta_{78} \gg T_K$, both in agreement with experiment. The CEF splitting comes from the larger Γ_7 -hybridization in the energy region from 1.0 to 3.0 eV, which results in the doublet (Γ_7) ground state for $\text{M}=\text{In, Pb}$. Naively, since $\Delta_{78} \sim V^2$, one would expect the larger crystal field splitting for CeIn_3 to correspond to a much larger T_K value than for CePb_3 which is not seen experimentally. This common reasoning assumes, however, energy independent hybridization, clearly not the case here as shown in FIG. 2. In detail, the hybridization strength averaged over energy of CeIn_3 exceeds that of CePb_3 which dictates $\Delta_{78}|\text{In} > \Delta_{78}|\text{Pb}$, while the smaller CeIn_3 hybridization near E_F yields a smaller T_K value. Apparently, detailed hybridization calculations are critical for *quantitative* understanding of real heavy fermion materials.

The *intermediate valence* materials, CeSn_3 and CePd_3 , have $\Delta_{78} \ll T_K$ due to their large hybridization, as shown in the table. This agrees with experiment which fails to resolve CEF peaks. For CePd_3 , the LDA yields an anomalously huge hybridization (up to 1.5 eV) between Pd- d and Ce- f orbitals below the Fermi energy, and as a result, the estimated T_K was nearly an order of magnitude larger than the experimental value [21].

The magnetic susceptibility $\chi(T)$ provides a measure of the degree of screening of the local moments by conduction electrons, for which we show our in FIG. 3(a). CeIn_3 and CePb_3 showed CEF effects at about 220 and 50 K, respectively, without sizable moment screening until the lowest accessible temperature. Starting with well-localized moment at high temperatures, $\chi(T)$ deviated from Curie-Weiss behavior; $\chi(T)$ of CeIn_3 crossed over from $|\frac{5}{2}; \Gamma_7 + \Gamma_8\rangle$ to $|\frac{5}{2}; \Gamma_7\rangle$ magnetic moment regime regaining inverse- T behavior at temperatures (10~100 K) well below the CEF splitting. For CePb_3 and CeIn_3 , the Kondo resonance peak begins to emerge (not shown here) near few K where the numerics of this

calculation becomes unstable.

For CeIn_3 , Lawrence *et al.* [16] interpreted the deviation of $\chi(T)$ from the Curie-Weiss behavior in the low temperature region as arising from spin-fluctuations with the characteristic temperature $T_{\text{sf}} \sim 50$ K. We believe that this effect is clearly from the CEF splitting ($\Delta_{78}=125$ K). The calculated T_K (few K) is much lower than CEF splitting and is inaccessible experimentally due to the onset of anti-ferromagnetism at 10 K. This CEF effect has been checked by comparing the experimental results with the Curie-Weiss susceptibility of Γ_7 - and Γ_8 -magnetic moments as well as the van Vleck susceptibilities. In particular, the experimental low temperature $\chi(T)$ curve shows saturates only below 10 K ($\ll T_{\text{sf}}$) and above this is well-fitted to the Curie-Weiss form with a characteristic temperature 18 K, which can be interpreted as a combination of Néel temperature plus the CEF effect from the excited quartet field Γ_8 .

In FIG. 3(b), susceptibility curves of CeSn_3 are plotted for several values of ϵ_f with a comparison to experiment [18]. Since $\chi(T \rightarrow 0)(\sim 1/T_K)$ is exponentially sensitive to ϵ_f (see Eq. (4)), we performed calculations for several ϵ_f 's ($-2.0, -2.1, -2.2$ eV). Clearly our calculations bracket but do not fit the experimental data. since a calculation for $\Delta_{78}=0$ fits the data well [22], we suspect the source of the disagreement may be an overestimate of crystal field splitting in our calculation, placing the effective degeneracy between two ($T_K \ll \Delta_{78}$) and six ($\Delta_{78} = 0$).

In conclusion, we reproduced both the band and many body features of the Ce-compounds by inputting LDA(LMTO-ASA) calculated hybridizations into $U \rightarrow \infty$ NCA calculations for appropriately defined impurity Anderson models. We reproduce well experimental trends in T_K , Δ_{78} , and $\chi(T)$ for the CeM_3 series. This work provides a starting point for quantitative calculations of realistic heavy fermion systems at finite temperatures. Improvement may come through a proper inclusion of f^2 dynamics ($U \neq \infty$), a reliable theory for electrostatic CEF contributions, and through self-consistent closure of the many body calculations.

We are grateful to J. W. Allen, M. Steiner and J. W. Wilkins for helpful discussions.

This work was supported by the United States Department of Energy, Office of Basic Energy Sciences, Division of Materials Research, and J.H. and D.L.C. acknowledge the support of NSF grant PHY94-07194 at the Institute for Theoretical Physics. Supercomputer time was provided by the Ohio Supercomputer Center.

REFERENCES

- [1] O. Gunnarsson and K. Schönhammer, Phys. Rev. B **28**, 4315 (1983).
- [2] N. E. Bickers, D. L. Cox, and J. W. Wilkins, Phys. Rev. B **36**, 2036 (1987).
- [3] J. M. Wills and B. R. Cooper, Phys. Rev. B **36**, 3809 (1987).
- [4] P. M. Levy and S. Zhang, Phys. Rev. Lett. **62**, 78 (1989).
- [5] M. Steiner, R.C. Albers, and L.J. Sham, Phys. Rev. Lett. **72**, 2923 (1994).
- [6] R. J. Birgeneau, *et al.* Phys. Rev. B **8**, 5345 (1973).
- [7] J. W. Allen, *et al.* Phys. Rev. Lett. **46**, 1100 (1981).
- [8] J. F. Herbst, R. E. Watson and J. W. Wilkins, Phys. Rev. B **13** (1976).
- [9] We chose the -2.0 eV value based upon the interconfiguration energy difference curves of Ref. [8] at the Wigner-Seitz cell value $r_{WS}(Ce)$ of elemental Ce. Our CeM₃ LDA r_{WS} values vary little from $r_{WS}(Ce)$ with M.
- [10] O. K. Andersen, Phys. Rev. B **12**, 3060 (1975).
- [11] We plot each atomic potential as a function of atomic radius and determine by inspection the ratio of the Wigner-Seitz radii of Ce and M when the potential becomes flat.
- [12] We explicitly checked that the hybridization is dominated by ligand(s, p for Pb, In, Sn or d for Pd)- $f(Ce)$ overlap. The Ce-Ce hopping ($d-f$, as well as $f-f$) is more than an order of magnitude smaller.
- [13] O. Jepsen and O. K. Andersen, Solid State Comm. **9**, 1763 (1971).
- [14] O. Gunnarsson, *et al.* Phys. Rev. B **39**, 1708 (1989).
- [15] A. Georges, G. Kotliar, W. Krauth, and M.J. Rozenberg, to be published in Rev. Mod. Phys. (1996) (cond-mat/9510091).

- [16] J. M. Lawrence, and S. M. Shapiro, Phys. Rev. B **22**, 4379 (1980).
- [17] C. L. Lin, *et al.* Phys. Rev. Lett. **58**, 1232 (1987), and references therein.
- [18] D. E. MacLaughlin, J. Mag. Mag. Mat. **47&48**, 121 (1985), and references therein.
- [19] The impurity limit calculation (FIG. 1 (b)) does not include the effect of f -orbital of La atoms which would reduce T_K due to the extra downward shift of the peak at -0.1 eV (inset of FIG. 2 (b)).
- [20] The (difficult) dynamic inclusion of finite U will modify T_K values due to the virtual exchange processes mediated by the f^2 configuration; practically, this will require recalibration of the ϵ_f values we input into the NCA.
- [21] The overestimated $\Gamma(\epsilon)$ values for CePd₃ may arise from the LDA underestimation of the $d(Pd)$ -band width.
- [22] E. Kim, and D. L. Cox, Phys. Rev. Lett. **75**, 2015 (1995).
- [23] V. T. Rajan, Phys. Rev. Lett. **51**, 308 (1983).

FIGURES

FIG. 1. Schematic diagrams of hopping of f -electrons to band states in $\text{Ce}_x\text{La}_{1-x}\text{M}_3$ systems. (a) In the $x = 1$ limit, the center f -orbital couples the rest of the lattice (enclosed in dashed line), *i.e.*, effective medium. The f -orbital is connected to ligand orbitals (c_i) with V_{im} (i lattice site, m the CEF index). The lattice of f orbitals (origin excluded) are treated as producing a *static* mean field coupling to ligands in the LDA calculation. (b) In the impurity limit ($x \rightarrow 0$), the f -orbital (at center) couples to the *bare* ligand bands.

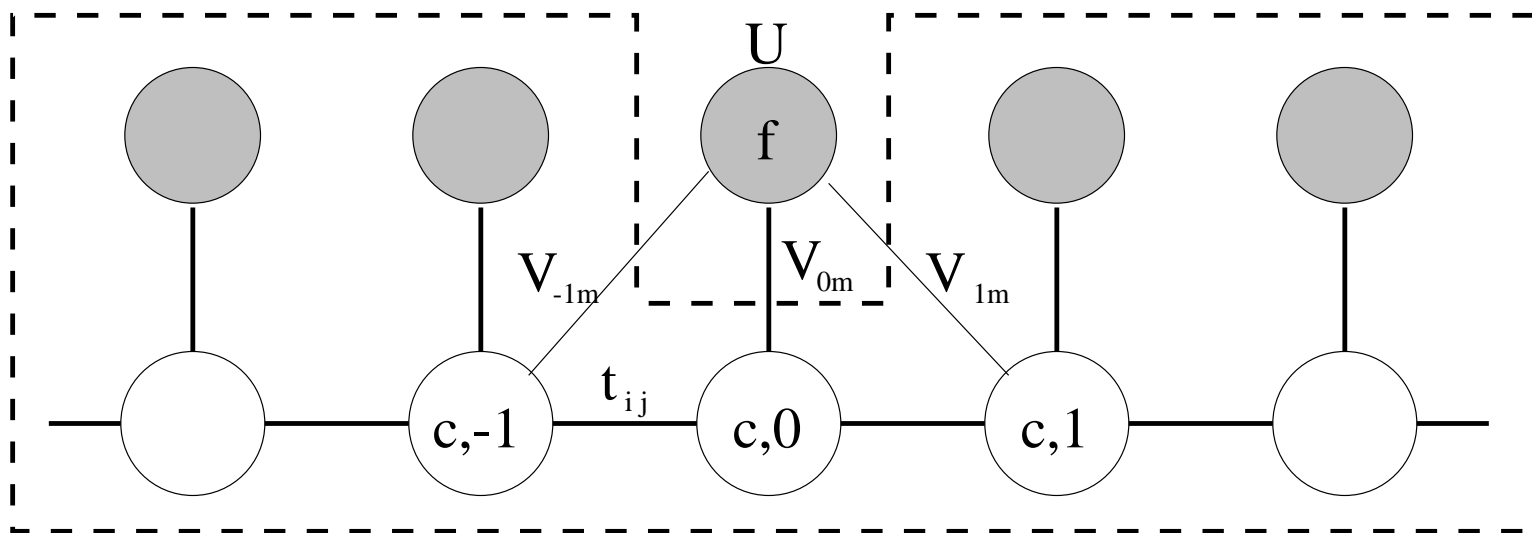
FIG. 2. Hybridizations of $\text{Ce}_x\text{La}_{1-x}\text{M}_3$ calculated in two different limits of x . (a) $x = 1$ limit. Although $\Gamma_7(J = 5/2)$ (thick line) and $\Gamma_8(J = 5/2)$ (thin line)-hybridizations are comparable, large hybridization ($f^1 \leftrightarrow f^0$ fluctuation) for Γ_7 near 1.0-3.0 eV pushes the doublet below the quartet. The spikes appearing above the Fermi energy (dashed line) are due to the coupling of f -orbital at origin to the bonding (anti-bonding) states of ligand and neighboring f -orbitals. (b) $x \rightarrow 0$ limit. Curves are almost identical to (a) except near the Fermi energy. Note that the peak at -0.1 eV (inset) is pushed down to -0.2 eV (inset (a)) due to f -ligand coupling.

FIG. 3. Calculated magnetic susceptibility $\chi(T)$ -vs.- T for CeM_3 compounds. (a) M dependence of $\chi(T)$; see text for discussion. (b) Magnetic susceptibilities of CeSn_3 for different f -level positions, ϵ_f .

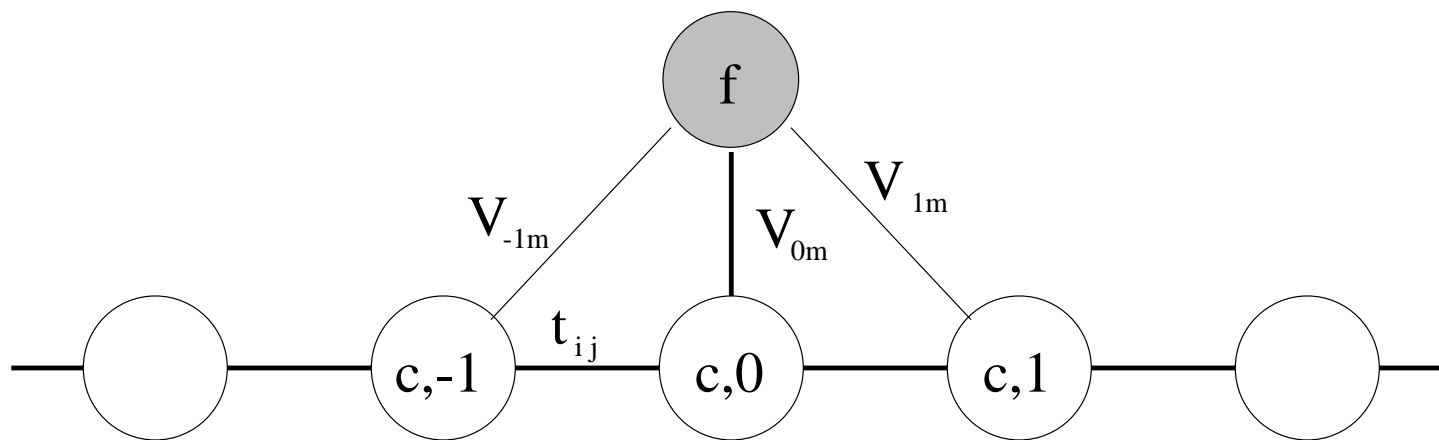
TABLES

TABLE I. Table of the electronic configuration of ligand atom M (E.C.) ground CEF multiplet Γ_{grd} , CEF splittings Δ_{78} and Kondo temperatures T_K for $\text{Ce}_x\text{La}_{1-x}\text{M}_3$ systems. Units are in Kelvin. Positive Δ_{78} indicates a stable Γ_7 ground doublet on the Ce sites. (*: For mixed valence systems, CEF's are not experimentally deducible since $\Delta_{78} \ll T_K$).

M	E.C.	Γ_{grd}	$\Delta_{78}^{\text{exp}}/T_K^{\text{exp}}$	$\Delta_{78}^{x=1}/T_K^{x=1}$	$\Delta_{78}^{x \rightarrow 0}/T_K^{x \rightarrow 0}$
Pb	$6s^2 6p^2$	Γ_7	67/3	50/(< 1)	40/23
In	$4d^{10} 5s^2 5p^1$	Γ_7	183/(< 11)	125/(< 1.0)	80/1.1
Sn	$4d^{10} 5s^2 5p^2$	Γ_7^*	-/450	159/400	176/238
Pd	$4d^{10}$	Γ_8^*	-/700	215/3210	314/2600



(a) concentrated limit (CeM_3)



(b) impurity limit ($\text{Ce}_x \text{La}_{1-x} \text{M}_3, x \geq 0$)

